ROBUST ULTRASONIC FLAW DETECTION USING ORDER STATISTIC CFAR THRESHOLD ESTIMATORS

J. SANIIE and D.T. NAGLE

Department of Electrical and Computer Engineering,
Illinois Institute of Technology, Chicago, IL 60616

ABSTRACT

Ultrasonic nondestructive imaging of critical defects (such as voids, microcracks, in bulk materials) is often hampered by the presence of interfering and random scatterers (i.e., clutter or grain echoes) associated with the defect's environment. The detection of broadband ultrasonic echoes for NDE can be improved by using optimal bandpass filtering to resolve flaw echoes surrounded by grain scatterers. The optimal bandpass filtering is achieved by examining spectral information of the flaw and the grain echoes where frequency differences have been experimentally shown to be predictable. The flaw echoes can then be discriminated by using adaptive thresholding techniques based on surrounding range cells. This paper presents Order Statistic (OS) Based processors (ranked and trimmed mean) to robustly estimate the threshold while censoring outliers. The design of these OS processors are accomplished analytically based on Constant False Alarm Rate (CFAR) detection. The OS Based CFAR detectors were evaluated using experimental data and their performance is compared with the Cell Averaging (CA) method. It is shown that the OS Based CFAR processors can detect flaw echoes robustly where the range cell used for the threshold estimate contains outliers.

INTRODUCTION

Ultrasonic flaw detection in large-grained materials is difficult since grain scattering echoes interfere with and sometimes mask flaw echoes. Therefore, signal processing methods are essential to enhance the defect's echo leading to reliable detection. Figure 1 shows an ultrasonic flaw detection system where the received ultrasonic signal is passed through a preprocessor for flaw-to-clutter ratio enhancement, and is then compared to an adaptive threshold for Constant False Alarm Rate (CFAR) detection. Enhancement of the flaw-to-clutter ratio is accomplished by preprocessing the signal utilizing differences in the frequency and statistical information of the flaw and grain echoes using optimal frequency ranges and order statistic processors. After preprocessing, the surrounding observations are used to create an adaptive threshold to allow for fluctuations in signal power. However, in certian instances, the existence of multiple flaws or high intensity noise information (i.e., outliers) requires a robust threshold estimate. Such threshold estimates can be obtained using order statistics which can censor extreme deviations from observations. Thus, the premise of this paper is twofold: (i) to develop and evaluate the effectiveness of preprocessing techniques for signal-to-clutter enhancement, and (ii) to analyze the design of CFAR detectors and their performance using experimental results.

In this paper, optimal bandpass filtering is utilized on the experimental data where the frequency characteristics of the flaw and grains are predicted using calibrated samples. An additional degree of improvement in resolution is achieved by applying Split-Spectrum Processing (SSP) such that all selected narrow frequency bands comprise regions of high flaw-to-clutter ratios [1-5]. The split spectrum technique provides a set of observations corresponding to different frequency bands which will decorrelate the microstructure noise. Furthermore, the performance of order statistic processors in conjunction with split spectrum processing technique is evaluated in the context of flaw-to-clutter enhancement and resolution [2,3].

From the preprocessed data, the presence of the flaw is then automatically determined using Constant False Alarm Rate (CFAR) detection. In this paper, several Order Statistic (OS) and Trimmed-Mean (TM) CFAR detectors

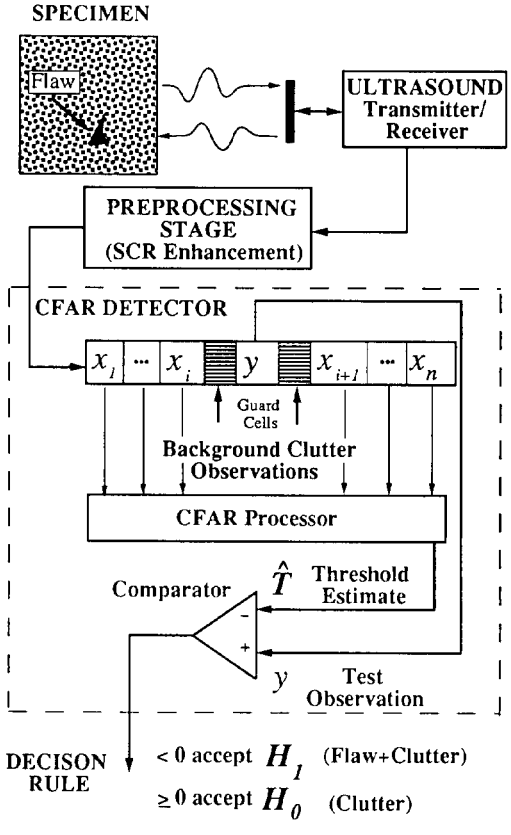

Figure 1. Block diagram of ultrasonic flaw detection system.

1051-0117/91/0000-0785 $1.00 © 1991 IEEE

are considered for robust threshold estimation. The design of these CFAR detectors is modeled and compared with the experimental results when the background observations are contaminated with flaw information.

FREQUENCY ANALYSIS OF ULTRASONIC BACKSCATTERED SIGNALS

The exploration of the frequency content of ultrasonic backscattered signals can give spectral energy profiles corresponding to the grains and the larger geometric reflectors (i.e., defects). The energy loss of ultrasonic signals is caused by the microstructure of the propagating media through which scattering and absorption occurs. The model for the overall frequency-dependent attenuation coefficient $\alpha(f)$ is defined as

$$\alpha(f) = \alpha_a(f) + \alpha_s(f), \tag{1}$$

where $\alpha_s(f)$ is the scattering coefficient and $\alpha_a(f)$ is the absorption coefficient.

The composite effects of scattering and attenuation due to grains can be characterized in terms of transfer functions derived from the spectrums of measured signals. The transfer function associated with the scattering and attenuation of the grains is evaluated experimentally using two type 1018 steel specimens (i.e., Sample I and Sample II) where Sample I was not heat-treated and Sample II has been heat-treated at a tempature of 1900^{o} F for 4hrs. The mean grain sizes of Samples I and II were found to be 14 and 50 microns, respectively. The backscattered ultrasonic signal and spectrum is shown in Figure 2 for different points in the steel blocks. Figure 2a shows the front surface echo, $r_f(t)$, and spectrum, $|R_f(f)|$ of the flat front surface of the steel block positioned in the far field of the transducer. This front surface echo represents the response of the transducer impulse function, $U(f)$,

$$|R_f(f)| \propto |U(f)| \tag{2}$$

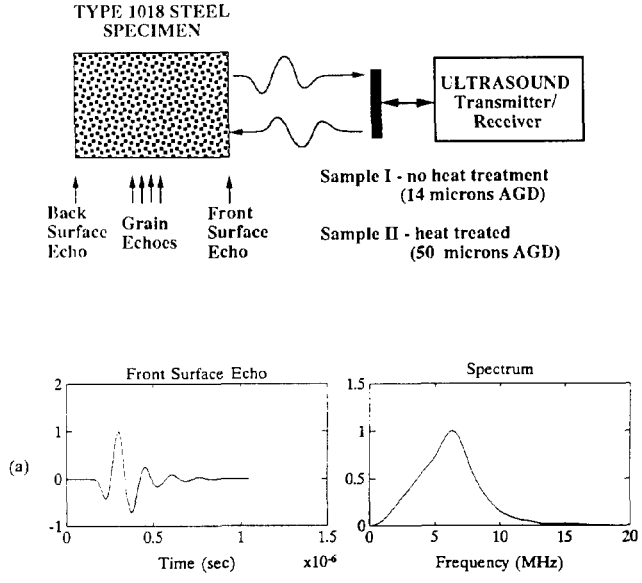

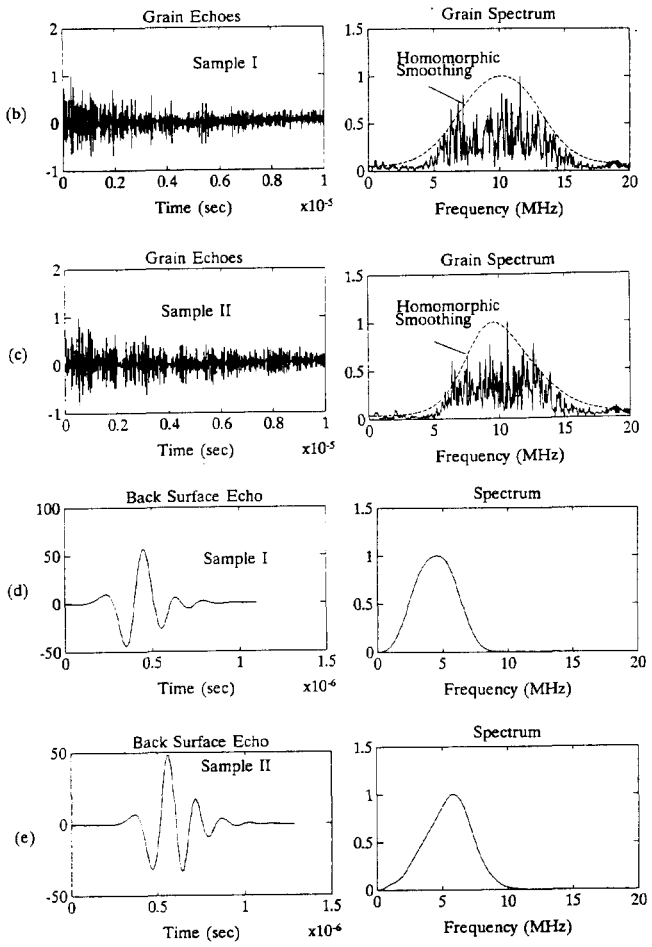

Figure 2. Ultrasonic measurements and spectrums at different points in steel samples I and II, displaying (a) a front surface echo (Sample I), (b) grain echoes of Sample I, and (c) grain echoes of Sample II, (d) a back surface echo of Sample I, and (e) a back surface echo of Sample II.

The effects of attenuation due to scattering and absorption of the propagating media are shown in Figures 2d and 2e where a flat back surface echo travels 20cm round trip into the steel samples I and II, respectively. The spectrum of the received signal, $R(f)$, can be modeled as:

$$|R_b(f)| \propto |A(f)|\ |U(f)| \tag{3}$$

where $A(f)$ is the transfer function corresponding to the attenuation characteristics of the signal propagation path. In Figure 3a, a heuristic evaluation of $|A(f)|$ is given by the ratio of the spectrums of the above measured signals, $|R_b(f)|/|R_f(f)|$. It can be seen that there is a definite shift or emphasis of the lower frequencies. This indicates that flaws significantly greater in size than the wavelength have dominant energy in lower frequencies.

The spectrum of the signal received from grains alone is shown in Figure 2b and 2c which can be modeled as follows:

$$|R_g(f)| \propto |A(f)|\ |S(f)|\ |U(f)|\ |G(f)| \tag{4}$$

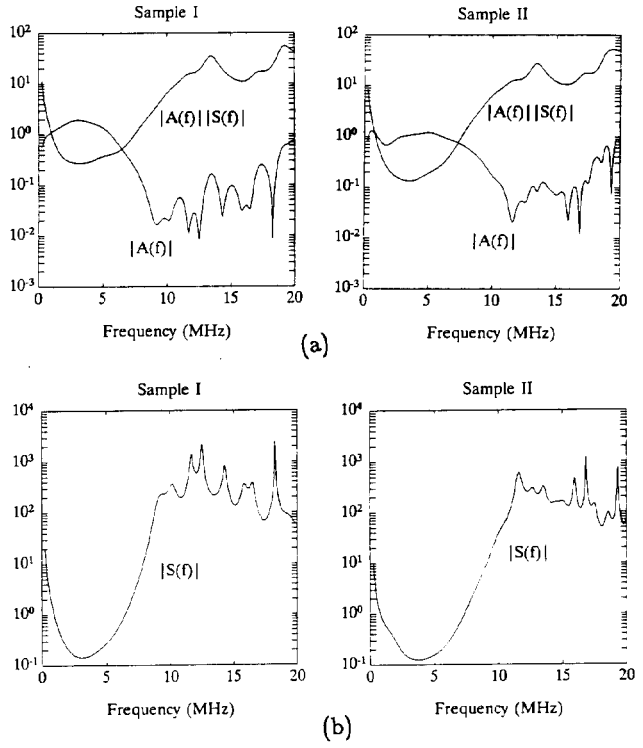

Figure 3. Scattering and attenuation transfer functions of ultrasonic measurements, where (a) shows $|A(f)|$ (i.e., $|R_b|/|R_f(f)|$) and $|A(f)||S(f)|$ (i.e., $|\tilde{R}_g(f)|/|R_f(f)|$) for Samples I and II, and (b) shows $|S(f)|$ (i.e., $|\tilde{R}_g(f)|/|R_b(f)|$) for Samples I and II.

where $|A(f)|$ is defined in Equation 3, $|S(f)|$ is the frequency-dependent scattering function [6], and $|G(f)|$ is a frequency modulation function due to the sum of small scatterers with random orientations and phases [6]. The function $G(f)$ causes sporadic cancellations of frequency components and consequently results in the noisey spectrum shown in Figure 2b and 2c. To eliminate the effect of $G(f)$, homomorphic spectral smoothing techniques [6] are employed in which the resulting spectrum, $\tilde{R}_g(f) \propto |A(f)|\,|S(f)|\,|U(f)|$, is shown in Figure 2b and 2c using a $28\,\mu sec$ shortpass lifter. The scattering function, $S(f)$, can be found by the ratios of the spectrums of the grain echoes (Equation 4) and the back surface echo (Equation 3), $\tilde{R}_g(f)/R_b(f)$, which is displayed in Figure 3b for steel samples I and II. These results indicate scattering causes the lower frequencies to become more severely attenuated resulting in an upward shift in the expected frequency of the grain spectrum. Both flaw and grains echoes display predictable frequency dynamics associated with the physical properties of the steel sample. These characteristics are advantageous and lead to obtaining optimal frequency range containing high flaw-to-clutter ratios for the SSP of the preprocessing stage.

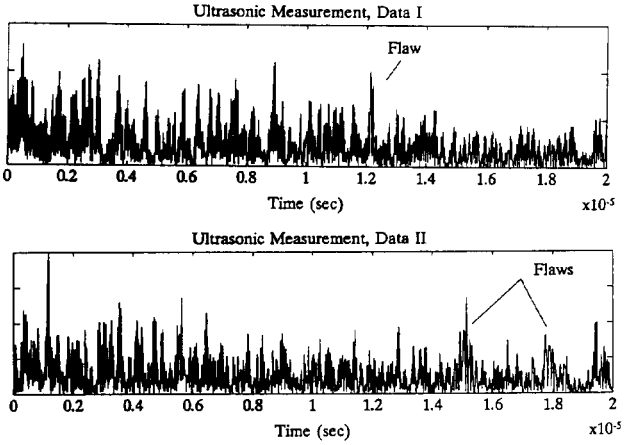

Figure 4. Experimental ultrasonic flaw measurements, where Data I has a single flaw reflector and Data II composed of two spatially-separated flaws.

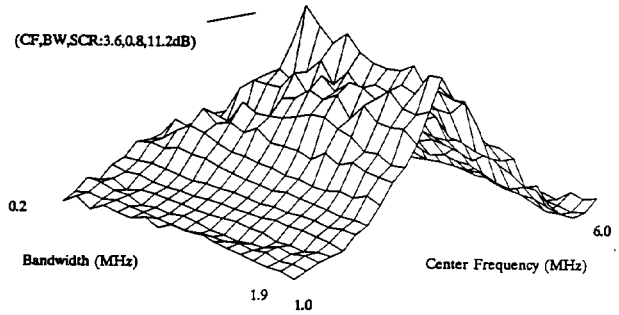

Figure 5. Flaw-to-clutter profiles of ideal bandpass (rectangular window) filtering with various center frequencies and bandwidths using Data I.

OPTIMIZED SPLIT SPECTRUM PROCESSING

It is critical to choose the parameters of the SSP appropriately in order to effectively enhance the flaw-to-clutter ratio [1-5]. The frequencies of the channels must reside within the information-bearing frequency range of the received signal, in particular, 2.5MHz−5MHz as shown in Figure 3b and 2. Also, the bandwidth of the channels must be large enough (0.5−1.0MHz) to maintain the resolution integrity of the echoes. These constraints limit the number of observations attainable without excessive frequency overlap between bands.

Figures 5 shows the flaw-to-clutter ratios profiles for various ideal bandpass filters in terms of center frequency and bandwidths for experimental measurement, referred to as Data I, shown in Figure 4. In Figure 5, the Data I set from Sample I indicates that the frequencies near 4MHz will give the best performance 0.8MHz or larger. Larger bandwidths are more robust since they will maintain the flaw information for shifts in different channels and also reduce the decorrelation of grain noise between channels. Since equivalent performance shown in Figure 3b the frequency differences due to grain size can be considered

insubstantial enough to significantly alter the SSP parameters. Therefore, using a typical specimen as the calibration tool for optimal frequency range is shown to be quite reliable.

Optimal SSP have been applied to several signals with various types of flaws in steel samples. Two experimental flaw measurements from steel samples I and II, is referred to Data I and Data II, respectively are shown in Figure 4 where Data I has a single simulated flaw (flat bottom hole) and Data III has two simulated flaws separated by $1.25cm$. The performance of the SSP with 11 channels of 1MHz 3dB-bandwidth equally-spaced between the frequency range of 3−5MHz using lower ranked order statistics (e.g., minimum) is shown in Figure 6. The next step is to utilize the SSP output in reliable detection of the presence and position of flaw echoes where the background clutter (i.e., grains) noise power fluctuates from region to region.

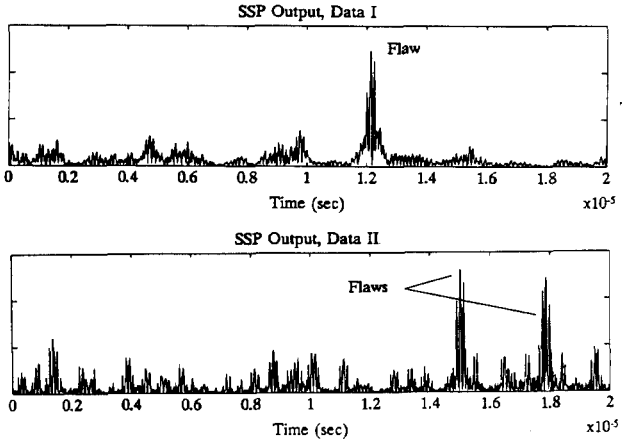

Figure 6. Optimal SSP outputs for Data I and II using minimum-ranked order statistics.

ADAPTIVE CFAR THRESHOLD ESTIMATORS

In ultrasonic systems, the effect of interfering echoes from the microstructure can degrade the detection of a flaw within a particular range cell. When the clutter distribution in a measurement is unknown, the performance of the optimal detector (i.e., Neyman-Pearson fixed-threshold detector) deteriorates significantly, and the need arises for a nonparametric or Constant False Alarm Rate (CFAR) detector which is designed to be insensitive to changes (e.g., power) in the density functions of the clutter. In this paper, OS-CFAR and TM-CFAR detectoors are implemented for different censoring scenarios, and their performance is compared with CA-CFAR using experimental data.

The threshold estimate for the CA-CFAR detector is given below:

$$\hat{T} = \theta \sum_{i=1}^{n} x_i \tag{5}$$

where θ is the scaling parameter, determined from the probability of false alarm.

The censored TM-CFAR threshold estimate corresponds to

$$\hat{T} = \theta \sum_{i=r+1}^{n-s} x_{(i)} \tag{6}$$

where r, s, are the number of smallest and largest censored observations, respectively, $x_{(i)}$ is the order statistic of rank i [7], and θ is the CFAR design parameter. This incorporates several order statistics which are combined linearly with equal weighting referred to the Trimmed-Mean (TM) CFAR detector.

The OS-CFAR the threshold is given by a scaled order statistic:

$$\hat{T} = \theta\, x_{(i)} \tag{7}$$

where this is the special case of the TM CFAR Detector when $r=i-1$ and $s=i+1$.

The design parameter, θ, of CA-CFAR [8], OS-CFAR [9] and TM-CFAR [10] detectors for exponentially-distributed observations can be found in a similar manner from Equation 11. The P_{FA} for the CA-CFAR detector is given by [8]:

$$P_{FA} = (1+\theta)^{-n}. \tag{8}$$

The P_{FA} for the TM-CFAR detector is given by [10]:

$$P_{FA} = \binom{n}{r}\binom{n-r}{s} \sum_{i=0}^{r} \frac{(-1)^{r-i}\binom{r}{i}}{(n-i)/(n-r-s)+\theta} \cdot \prod_{k=2}^{n-r-s} \left[\frac{n-r-k+1}{n-r-s-k+1} + \theta\right]^{-1} \tag{9}$$

The P_{FA} for the OS-CFAR detector is given by [9]:

$$P_{FA} = i\binom{n}{i} \mathrm{B}(i, n-i+\theta+1) = \frac{n!\,\Gamma(n-i+\theta+1)}{(n-i)!\,\Gamma(n+\theta+1)} \tag{10}$$

where $\mathrm{B}(\cdot)$ and $\Gamma(\cdot)$ are Beta and Gamma functions [11], respectively.

CFAR FLAW DETECTION - EXPERIMENTAL RESULTS

To implement the CFAR detector effectively, the parameters of the detector must be chosen in accordance with the resolution of the flaw echoes and the number of flaws present. For this study, experimental measurements (Figure 4) and SSP outputs (Figure 6) are used to illustrate different flaw scenarios where the preprocessed signals have comparable flaw-to-clutter ratios of approximately 11dB. In Figure 6a, the signal shows a flaw from a single reflector. The case where two resolvable flaws are present is shown in Figure 6b. These cases will be applied to the previously-mentioned CFAR processors where the parameters are chosen to provide robust performance at equivalent levels of probability of false alarm.

Since only one observation is used for testing (i.e., flaw information), the resolution of the flaw echoes requires guard cells to seperate the samples containing concurrent flaw information from the threshold estimate which is based on the background clutter observations. The resolution of this system for the transducer center frequency of 7MHz and 3dB-bandwidth of about 3MHz and sampling rate of 100MHz is approximately 25 samples. An example of the performances of OS, TM, and CA-CFAR detectors for Data I is given in Figure 7 for $n=128$ and number of guard cells equal to 64 which is at least twice the duration of a single echo. This figure indicates that the guard cells maintain comparable clutter threshold levels for all detectors in the region of the flaw, however, the presence of the two large peaks on either side of the flaw will prevent

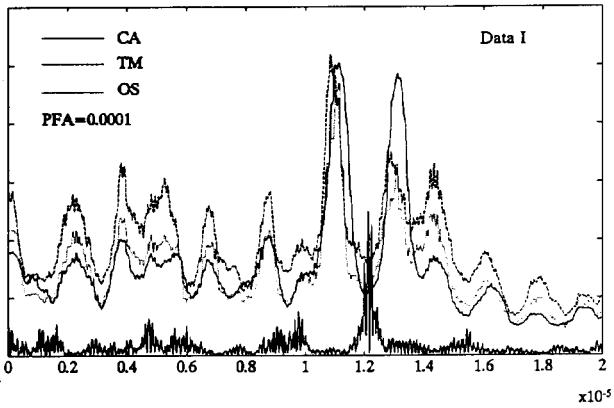

Figure 7. Adaptive threshold performance for OS, TM, and CA CFAR detectors for $P_{FA}=10^{-4}$ and parameters: $n=128$, $i=64$, $r=0$, and $s=64$ using Data I.

detection of other potential flaws in that region when multiple flaws occur. Figure 7 illustrates that the censoring properties of the OS ($i=64$) and TM-CFAR ($s=64$ & $r=0$) detectors reduce the effect of contaminating flaw information. It should be noted that the scaling factors derived from Equations 8-10 assume that the clutter observations are exponentially-distributed in which deviations in the probability of false alarm may exist. The performance of the OS in this instance shows lower levels than the TM threshold, however the TM threshold has less variations, hence the TM threshold would perform with a lower incident of false alarm.

For the Data II, where multiple flaws are present, Figure 8 shows the case where CA fails to detect flaw echoes due to contamination. In this example, the clutter window length is 256 samples, guard cells of 344, OS threshold with $i=192$, TM thershold with $s=64$ and $r=0$, and $P_{FA}=10^{-5}$. In contrast to the performance of the CA-CFAR detector, both the OS and TM CFAR thresholds are able to detect flaw echoes.

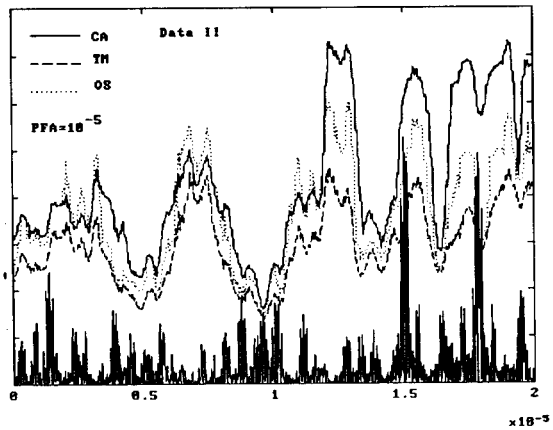

Figure 8. Adaptive threshold performance for OS, TM, and CA CFAR detectors for $P_{FA}=10^{-5}$ and parameters: $n=256$, $i=192$, $r=0$, and $s=64$ using Data II.

CONCLUSIONS

In this paper, we have presented a theory and application of SSP and CFAR detectors in ultrasonic flaw detection. The theory suggests that the optimal SSP can be found upon the knowledge of frequency ranges containing high flaw-to-clutter ratios which can be determined through calibration. We have shown through experimental results that lower ranks order statistics applied to SSP perform well in terms of enhancing the flaw-to-clutter ratio and flaw resolution. Furthermore, the adaptive threshold has shown to maintain CFAR performance when the *a priori* knowledge of the distributions is incomplete. This paper introduces the application of CA, OS, TM-CFAR threshold estimators for flaw detection. These estimators have been applied to experimental data and results indicate that for the case of multiple targets, the OS, and TM-CFAR detectors show more robust performance over the CA-CFAR Detector. Therefore, it is recommended using CFAR threshold estimators based on order statistics to censor outliers and to increase the probability of detection.

ACKNOWLEDGEMENTS

This work was supported by SDIO/IST funds managed under contract no. S40000RB01 by the Office of Naval Research, and Electric Power Research Institute, RP 2405-22.

REFERENCES

[1] R. Murthy, N. Bilgutay and J. Saniie, "Application of Bandpass Filtering in Ultrasonic Non-Destructive Testing", *Quant. NDE of Materials,* Plenum Press, vol. 8, pp. 759-767, 1989.

[2] J. Saniie, D.T. Nagle, and K.D. Donohue, "Analysis of Order Statistic Filters Applied to Ultrasonic Flaw Detection using Split-Spectrum Processing," *IEEE Trans. on UFFC,* Vol. 38, No. 2, pp. 133-140, March 1991.

[3] N.M. Bilgutay and J. Saniie, "The Effect of Grain Size on Flaw Visibility Enhancement Using Split-Spectrum Processing," *Materials Evaluation,* Vol. 42, pp. 808-814, May 1984.

[4] V. L. Newhouse, N. M. Bilgutay, J. Saniie, E. S. Furgason, "Flaw-to-Grain Echo Enhancement by Split-Spectrum Processing" *Ultrasonics,* pp. 59-68, March 1982.

[5] J. Saniie, T. Wang, and N.M. Bilgutay, "Optimal Ultrasonic Flaw Detection Using a Frequency Diversity Techniques," *Review of Progress in Quant. Nondestructive Evaluation,* edited by D.O. Thompson and D.E. Chimenti, Vol. 8A, pp. 751-758, Plenum Press, New York, 1989.

[6] J. Saniie, T. Wang, and N.M. Bilgutay, "Analysis of Homorphic Processing for Ultrasonic Grain Signal Characterizations", *Transactions on UFFC,* pp. 365-375, May 1989.

[7] H. A. David, I. Order Statistics, John Wiley and Sons, Inc., New York, 1981.

[8] H.M. Finn, and R.S. Johnson, "Adaptive detection mode with threshold control of spatially sampled clutter-level estimates," *RCA Rev.,* Vol. 30, pp. 414-465, Sept. 1968.

[9] H. Rohling, "Radar CFAR Thresholding in Clutter and Multiple Target Situations," *IEEE Trans. on Aerospace and Electronic Systems,* vol. 19, pp. 608-621, July 1983.

[10] P.P. Gandhi and S.A. Kassam, "Analysis of CFAR Processors in Nonhomogeneous Background," *IEEE Trans. on Aerospace and Electronic Systems,* AES-24, no. 4, pp. 427-445, 1988.

[11] M. Abramowitz, and I.A. Stegun, *Handbook of Mathematical Functions,* National Bureau of Standards Applied Mathematics Series, no. 55, Government Printing Office, Washington D.C., 1964.